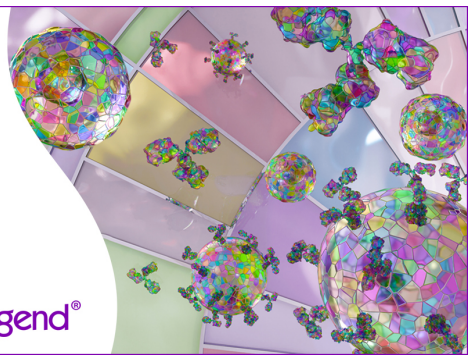

The Journal of Immunology
RESEARCH ARTICLE | MARCH 27 2023

African Swine Fever Virus HLJ/18 CD2v Suppresses Type I IFN Production and IFN-Stimulated Genes Expression through Negatively Regulating cGMP-AMP Synthase–STING and IFN Signaling Pathways FREE

Li Huang; ... et. al

J Immunol (2023) 210 (9): 1338–1350.
https://doi.org/10.4049/jimmunol.2200813

African Swine Fever Virus HLJ/18 CD2v Suppresses Type I IFN Production and IFN-Stimulated Genes Expression through Negatively Regulating cGMP-AMP Synthase–STING and IFN Signaling Pathways

Li Huang,*,†,[1] Weiye Chen,*,[1] Hongyang Liu,*,[1] Mengdi Xue,*,[1] Siqi Dong,* Xiaohong Liu,* Chunying Feng,* Shinuo Cao,*,‡ Guangqiang Ye,* Qiongqiong Zhou,* Zhaoxia Zhang,*,† Jun Zheng,*,† Jiangnan Li,*,† Dongming Zhao,* Zilong Wang,* Encheng Sun,* Hefeng Chen,* Shuai Zhang,* Xue Wang,* Xianfeng Zhang,* Xijun He,* Yuntao Guan,* Zhigao Bu,* and Changjiang Weng,*,†

African swine fever is a fatal infectious disease caused by African swine fever virus (ASFV). The high mortality caused by this infectious disease is a significant challenge to the swine industry worldwide. ASFV virulence is related to its ability to antagonize IFN response, yet the mechanism of antagonism is not understood. Recently, a less virulent recombinant virus has emerged that has a EP402R gene deletion within the parental ASFV HLJ/18 (ASFV-ΔEP402R) strain. EP402R gene encodes CD2v. Hence we hypothesized that ASFV uses CD2v protein to evade type I IFN–mediated innate immune response. We found that ASFV-ΔEP402R infection induced higher type I IFN response and increased the expression of IFN-stimulated genes in porcine alveolar macrophages when compared with parental ASFV HLJ/18. Consistent with these results, CD2v overexpression inhibited type I IFN production and IFN-stimulated gene expression. Mechanistically, CD2v, by interacting with the transmembrane domain of stimulator of IFN genes (STING), prevented the transport of STING to the Golgi apparatus, and thereby inhibited the cGMP-AMP synthase–STING signaling pathway. Furthermore, ASFV CD2v disrupted IFNAR1-TYK2 and IFNAR2-JAK1 interactions, and thereby inhibited JAK-STAT activation by IFN-α. In vivo, specific pathogen-free pigs infected with the mutant ASFV-ΔEP402R strain survived better than animals infected with the parental ASFV HLJ/18 strain. Consistent with this finding, IFN-β protein levels in the peripheral blood of ASFV-ΔEP402R–challenged pigs were significantly higher than in the blood of ASFV HLJ/18–challenged pigs. Taken together, our findings suggest a molecular mechanism in which CD2v inhibits cGMP-AMP synthase–STING and IFN signaling pathways to evade the innate immune response rendering ASFV infection fatal in pigs. ***The Journal of Immunology*****, 2023, 210: 1338–1350.**

African swine fever (ASF) is a severe animal infectious disease caused by ASF virus (ASFV), and the morbidity and mortality of pigs infected with virulent ASFV isolates are as high as 100% (1). ASF has spread into many areas of the world, which has been threatening the world's pig factories with huge economic and ecological consequences (2). ASFV is a large, enveloped dsDNA virus. The genome of ASFV ranges in length from ∼170 to 190 kb depending on the virus strains (3). Normally, the ASFV genome contains between 151 and 167 open reading frames, which encode >150 proteins (4). Besides the structural proteins dedicated to viral entry, virus replication, and assembly, the ASFV genome also encodes many nonessential proteins that play important roles in evading host antiviral immune responses (5), including inhibition of type I IFN production (6–10) and NLRP3-dependent inflammatory response (9). Until now, about half of ASFV genes lacked any known or predictable functions.

On DNA viral infection, cGMP-AMP (cGAMP) synthase (cGAS) recognizes viral dsDNA and uses ATP and GTP to synthesize the

*Division of Fundamental Immunology, National African Swine Fever Para-reference Laboratory, State Key Laboratory of Veterinary Biotechnology, Harbin Veterinary Research Institute, Chinese Academy of Agricultural Sciences, Harbin, China; †Heilongjiang Provincial Key Laboratory of Veterinary Immunology, Harbin, China; and ‡Jiangsu Agri-Animal Husbandry Vocational College, Veterinary Bio-Pharmaceutical, Jiangsu Key Laboratory for High-Tech Research and Development of Veterinary Biopharmaceuticals, Taizhou, China

[1]L.H., W.C., H.L., and M.X. contributed equally to this work.

ORCIDs: 0000-0002-4750-2329 (E.S.); 0000-0003-2245-1032 (H.C.); 0000-0002-7403-7899 (X.Z.); 0000-0002-7676-9030 (C.W.).

Received for publication November 4, 2022. Accepted for publication February 24, 2023.

This work was supported by the National Natural Science Foundation of China (Grants 32270156 and U21A20256), Natural Science Foundation of Heilongjiang Province of China (Grant YQ2020C022), and Jiangsu Province Key Research and Development Program (modern Agriculture) project (Grant BE2020407).

Address correspondence and reprint requests to Prof. Changjiang Weng and Zhigao Bu, Division of Fundamental Immunology, National African Swine Fever Para-reference Laboratory, State Key Laboratory of Veterinary Biotechnology, Harbin Veterinary Research Institute, Chinese Academy of Agricultural Sciences, Harbin 150069, China. E-mail addresses: wengchangjiang@caas.cn (C.W.) and buzhigao@caas.cn (Z.B.)

The online version of this article contains supplemental material.

Abbreviations used in this article: ABZI, amidobenzimidazole; ASF, African swine fever; ASFV, African swine fever virus; CBD, CDN-binding domain; cGAMP, cGMP-AMP; cGAS, cGMP-AMP synthase; Co-IP, coimmunoprecipitation; DEG, differentially expressed gene; diABZI, diamidobenzimidazole; dpi, days postinoculation; ER, endoplasmic reticulum; HA, hemagglutinin; HAD_{50}, 50% hemadsorption dose; hpi, hours postinfection; ISRE, IFN stimulus response element; IRF3, IFN regulatory factor 3; ISG, IFN-stimulated gene; KEGG, Kyoto Encyclopedia of Genes and Genomes; MOI, multiplicity of infection; pAb, polyclone Ab; PAM, pulmonary alveolar macrophage; qPCR, quantitative real-time PCR; RNA-seq, RNA sequencing; SPF, specific pathogen-free; STING, stimulator of IFN genes; TK, thymidine kinase; TM, transmembrane domain; WT, wild type.

second messenger cGAMP (11, 12). cGAMP binds to stimulator of IFN genes (STING), which causes a conformational change of STING and then translocates from the endoplasmic reticulum (ER) to the Golgi apparatus (13, 14). Subsequently, STING recruits and phosphorylates TBK1, and the active TBK1 phosphorylates IFN regulatory factor 3 (IRF3), leading to its translocation to the nucleus. IRF3 binds to IFN promoter and initiates transcription of type I IFNs (15, 16). Type I IFN binds to its receptors (IFNAR1/IFNAR2) and then recruits IFN receptor–associated JAK1 and TYK2. The activated JAK1 and TYK2 phosphorylate STAT1 and STAT2, which leads them to transport into the nucleus to promote IFN-stimulated gene (ISG) expression (17).

ASFV CD2v, encoded by EP402R gene, is a late-expressed viral glycoprotein during ASFV infection. It resembles the adhesion receptor CD2, which is expressing on the surface of T lymphocyte and NK cells (18). ASFV CD2v is located around viral factories during ASFV infection, and it is required for the hemadsorption of RBCs around ASFV-infected cells (19). ASFV CD2v can be cleaved in the ER or Golgi compartments to produce N-terminal fragment with glycosylation and C-terminal fragment with nonglycosylation (20). It has been reported that ASFV CD2v interacts with actin-binding adaptor protein SH3P7 and adaptor protein AP1 (21, 22). The functions of ASFV CD2v are also involved in tissue tropism, cell–cell adhesion (23), viral virulence immune evasion (18), viral replication (24), and the pathogenesis of ASFV (25). ASFV CD2v can damage the function of lymphocytes, and the expression of CD2v has some connection with ASFV spreading in domestic swine. Recently, ASFV CD2v was found to induce NF-κB–dependent IFN-β and ISGs transcription in swine PK15 cells. ASFV CD2v interacts with CD58 and induces apoptosis of PBMCs and macrophages (26). However, to date, the functions of CD2v in regulating type I IFN production and its downstream signaling have not been investigated yet.

In this study, we report that ASFV CD2v is an inhibitor in modulating type I IFN production and ISG expression by antagonizing cGAS-STING and IFN signaling pathways. ASFV CD2v inhibits the STING translocation to the Golgi apparatus through interaction with the transmembrane domain (TM) of STING. ASFV CD2v also inhibits ISG production by disrupting the interactions of IFNAR1-TYK2 and IFNAR2-JAK1. Compared with ASFV HLJ/18, a recombinant ASFV with deletion of EP402R gene from ASFV HLJ/18 (ASFV-ΔEP402R) infection enhances host antiviral innate immune responses, resulting in reducing the pathogenicity of ASFV. Our findings provide a new clue to explain how ASFV CD2v is related to the pathogenicity of ASFV.

Materials and Methods

Ethics statement

This study was carried out following the Guide for the Care and Use of Laboratory Animals of the Ministry of Science and Technology of the People's Republic of China. The protocols were approved by the Committee on the Ethics of Animal Experiments of the Harbin Veterinary Research Institute of the Chinese Academy of Agricultural Sciences and the Animal Ethics Committee of Heilongjiang Province, China.

Biosafety statement and facility

All experiments with live ASFV were conducted within the enhanced biosafety level 3 (P3+) and level 4 (P4) facilities in the Harbin Veterinary Research Institute of the Chinese Academy of Agricultural Sciences approved by the Ministry of Agriculture and Rural Affairs and China National Accreditation Service for Conformity Assessment.

Reagents and Abs

The protein A/G-agarose used for coimmunoprecipitation (Co-IP) was purchased from Santa Cruz Biotechnology (20397; Dallas, TX). The cGAMP (SML1232), polyinosinic-polycytidylic acid [poly(I:C)] (31852-29-6), rabbit anti-Flag (F7425), mouse anti-Flag (F1804), rabbit anti-hemagglutinin (anti-HA; SAB4300603), and mouse anti-HA (H9658) Abs were purchased from Sigma-Aldrich (St. Louis, MO). The following Abs were purchased from Cell Signaling Technology (Danvers, MA): anti-JAK1 (29261S), anti-TYK2 (14193S), anti-STAT1 (14994S), anti-STAT2 (72604S), anti–STAT1-p (9167S), and anti–STAT2-p (88410S) Abs. Anti-GFP (50430-2-AP) polyclone Ab (pAb) was purchased from Proteintech (Wuhan, China). Mouse anti-CD2v and anti-p54 pAbs were produced in mouse by immunization with recombinant ASFV CD2v and p54. Mouse anti-STING and rabbit anti-STING pAbs were produced in mouse and rabbit by immunization with recombinant pig STING protein, respectively. Anti-mouse IgG (H+L) DyLight 800-Labeled (042-07-18-06) was purchased from Sera Care (Milford, MA). The IRDye 800CW goat anti-rabbit IgG secondary Ab (926-32211) was purchased from LI-COR (Lincoln, NE).

Plasmids and cells

The IFN-β reporter, IFN stimulus response element (ISRE) reporter, and thymidine kinase (TK)-Renilla reporter were presented from Prof. Hong Tang. The ASFV HLJ/18 strain was isolated from a pig sample in a farm of northeastern China during the ASF outbreak in 2018 (27). The ASFV EP402R cDNA was synthesized based on the genome of ASFV HLJ/18 isolate and cloned into pCAGGS-Flag vector from GenScript (Nanjing, China). To construct plasmids expressing Flag-tagged or HA-tagged cGAS, STING, TBK1, IRF3, IFNAR1, IFNAR2, JAK1, TYK2, STAT1, STAT2, and IRF9, we amplified the cDNAs corresponding to these swine genes by standard RT-PCR using total RNA extracted from porcine alveolar macrophages (PAMs) as templates and then cloned them into the pCAGGS-Flag or pCAGGS-HA vector, respectively. All constructs were validated by DNA sequencing. The primers used in this study are listed in Table I. HEK293T and MA104 cell lines were purchased from ATCC and cultured in DMEM, and PAMs isolated from specific pathogen-free (SPF) piglets (without ASFV, porcine reproductive and respiratory syndrome virus, pseudorabies virus, porcine circovirus type 2 and other 28 pathogens) were cultured in RPMI 1640 supplemented with 10% FBS, 100 U/ml penicillin, and 100 μg/ml streptomycin at 37°C with 5% CO_2.

Hemadsorption assay

In brief, PBMCs isolated from SPF piglets were seeded in 96-well plates and then were infected with 0.1 ml/well 10-fold serially diluted supernatant in quintuplicate. The quantity of ASFV was determined by identification of characteristic rosette formation representing hemadsorption of erythrocytes around ASFV-infected cells. At 7 d postinfection, the 50% hemadsorption doses (HAD_{50}s) were determined by the Reed–Muench method. All data are shown as the means of three independent experiments.

Co-IP and immunoblot analysis

Co-IP and immunoblot analysis were performed as previously described (28). In brief, for Co-IP, whole-cell extracts were lysed in lysis buffer (50 mM Tris-HCl [pH 7.4], 150 mM NaCl, 5 mM $MgCl_2$, 1 mM EDTA, 1% Triton X-100, and 10% glycerol) containing 1 mM PMSF and a 1× protease inhibitor mixture (Roche). Then, cell lysates were incubated with anti-Flag (M2) agarose or with protein G Plus-Agarose immunoprecipitation reagent (Santa Cruz Biotechnology) together with 1 μg of the corresponding Abs at 4°C overnight on a roller. The precipitated beads were washed five times with cell lysis buffer. For immunoblot analysis, equal amounts of cell lysates and immunoprecipitants were resolved by 10–12% SDS-PAGE and were then transferred to a polyvinylidene difluoride membrane (Millipore). After incubation with primary and secondary Abs, the membranes were visualized by ECL (Thermo Fisher Scientific) or an Odyssey two-color infrared fluorescence imaging system (LI-COR).

Confocal microscopy

MA104 cells transfected with the indicated plasmids were fixed for 20 min in 4% paraformaldehyde in 1× PBS at pH 7.4. The fixed cells were permeabilized for 20 min with 0.3% Triton X-100 in 1× PBS and were then blocked in 1× PBS with 10% BSA for 30 min. The cells were incubated with the appropriate primary Abs and were then stained with Alexa Fluor 594–labeled goat anti-mouse IgG and Alexa Fluor 488–labeled goat anti-rabbit IgG. The subcellular localization of indicated proteins was visualized using a Zeiss LSM-880 laser scanning fluorescence microscope (Carl Zeiss, Oberkochen, Germany) under a 63× oil objective.

Luciferase reporter assay

Luciferase activities were measured with a Dual-Luciferase Reporter Assay System (Promega) according to the manufacturer's instructions. The data were normalized to the transfection efficiency by dividing the firefly luciferase activity by the Renilla luciferase activity.

Table I. Primers used for PCR in this study

Plasmids	Primers (5′-3′)
pCAGGS-HA-cGAS	F: 5′-CCGGAATTCGCAGACTCTTGTGTGCCCGC-3′
	R: 5′-CGGGGTACCAAAAATTCAACTCCAATTTATTC-3′
pCAGGS-HA-STING	F: 5′-CCGGAATTCATGCCCCACTCCAGCCTGCAT-3′
	R: 5′-CGGGGTACCTCAAGAGAAATCCGTGCGGAG-3′
pCAGGS-HA-TBK1	F: 5′-CCGGAATTCATGCAGAGCACTTCTAATCATCTTTGG-3′
	R: 5′-CGGGGTACCCTAAAGACAGTCAACATTGCGAAGGC-3′
pCAGGS-Flag-IFNAR1	F: 5′-ATGCTCGGGCTTCTGGGTGC-3′
	R: 5′-TCACACGGCTGCCTGTCGCAGAA-3′
pCAGGS-Flag-IFNAR2	F: 5′-ATGCTTTTGAGCCAGAATGTCTCCG-3′
	R: 5′-TCATCTCATGATATATCCATCCC-3′
pCAGGS-Flag-JAK1	F: 5′-ATGGCTTTTTGTGCTAAAA-3′
	R: 5′-TTATTTTAAAAGTGCTT-3′
pCAGGS-Flag-Tyk2	F: 5′-ATGCCTCTGTGCCATTGGGGAGC-3′
	R: 5′-TCAGCAGACACTGAACACTGAG-3′
pCAGGS-Flag-STAT1	F: 5′-ATGTCCCAGTGGTATGAGCT-3′
	R: 5′-TTAGTCAAGGTTCATAGTTCCAG-3′
pCAGGS-Flag-STAT2	F: 5′-ATGGCGCAGTGGGAGATGC-3′
	R: 5′-CTAGTAGTCAGAAGGAATC-3′
pCAGGS-Flag-IRF9	F: 5′-ATGGCTTCAGGCAGGGCTCG-3′
	R: 5′-TCAAAGCAGATAGGAGGAGCA-3′
pCAGGS-Flag-EP402R	F: 5′-GAATTCGAGCTCATCGATGGTACCGGTACCATGATCATTCTGA-3′
	R: 5′-TTAATTAAGATCTGCTAGCTCGAGGGTACCGATAATCCGGTCC-3′
pCAGGS-Flag-EP402R-N	F: 5′-GAATTCGAGCTCATCGATGGTACCATGATCATTCTGATTTTCCTGA-3′
	R: 5′-TTAATTAAGATCTGCTAGCTCGAGGGTACCCAGGAAGGTGATGA-3′
pCAGGS-Flag-EP402R-C	F: 5′-GAATTCGAGCTCATCGATGGTACCTCCCTGCGCAAGAGAAAG-3′
	R: 5′-TTAATTAAGATCTGCTAGCTCGAGGATAATCCGGTCCACGTGGATCA-3′
pCAGGS-HA-STING-D1	F: 5′-TTCGAGCTCATCGATGGTACCATGCCCTACTCCAGCCTGCATCCA-3′
	R: 5′-ATTAAGATCTGCTAGCTCGAGGAGTACGTTCTTGTGGCGCTGAT-3′
pCAGGS-HA-STING-D2	F: 5′-TTCGAGCTCATCGATGGTACCATGCCCTACTCCAGCCTGCATCCA-3′
	R: 5′-ATTAAGATCTGCTAGCTCGAGCTCCCTTTCCTCCTGCCGAAGGTG-3′

F, forward; R, reverse.

Quantitative real-time PCR

To detect mRNA levels of IFN-β, we extracted total RNA using TRIzol reagent (Invitrogen), and reverse transcription was performed with a PrimeScript RT Reagent Kit (Takara). Reverse transcription products were amplified using an Agilent-Strata gene Mx Real-Time qPCR (quantitative real-time PCR) system with SYBR Premix Ex Taq II (Takara) according to the manufacturer's instructions. Data were normalized to the level of β-actin expression in each individual sample. For ASFV genomic DNA detection, ASFV genomic DNA was extracted by using QIAamp DNA Mini Kit (Qiagen, Germany). qPCR was carried out on a QuantStudio5 system (Applied Biosystems) according to the World Organization for Animal Health-recommended procedure described by King et al. (29). All the qPCR primers are listed in Table II.

Generation of ASFV-ΔEP402R recombinant virus

ASFV-ΔEP402R, a recombinant virus with deletion of EP402R gene, was generated by homologous recombination in PAMs. Recombinant transfer vector (p72-EGFP) containing a reporter gene cassette containing the EGFP gene with the ASFV p72 late gene promoter, two DNA fragments mapping ~500 bp to the left and right of EP402R gene, were used. PAMs were transfected with the linearized transfer vector using FuGENE HD following the manufacturer's protocol. Twenty-four hours after transfection, cells were infected with ASFV HLJ/18 for another 24 h. A recombinant ASFV-ΔEP402R was purified by fluorescent plaque five times and confirmed by sequencing.

RNA sequencing analysis

PAMs were infected with ASFV HLJ/18 or ASFV-ΔEP402R (multiplicity of infection [MOI] = 1) for 24 h, and then the total RNA was extracted. A total amount of 2 μg RNA per sample was used as input material for the RNA sample preparations. Sequencing libraries were generated using NEBNext Ultra RNA Library Prep Kit for Illumina (#E7530L; NEB) following the manufacturer's recommendations. The reference genomes and the annotation file were downloaded from ENSEMBL database (http://www.ensembl.org/index.html). Bowtie2 v2.2.3 was used for building the genome index, and clean data were then aligned to the reference genome using HISAT2 v2.1.0. Reads count for each gene in each sample was counted by HTSeq v0.6.0, and fragments per kilobase million mapped reads were then calculated to estimate the expression level of genes in each sample. Genes with $q \leq 0.05$ and $|\log2\_ratio| \geq 1$ are identified as differentially expressed genes (DEGs). For the functional enrichment of DEGs, the Kyoto Encyclopedia of Genes and Genomes (KEGG) enrichment of DEGs was performed by KOBAS online analyses (http://kobas.cbi.pku.edu.cn/), in which the p value was adjusted by multiple comparisons as q value. KEGG terms with $q < 0.05$ were considered to be significantly enriched.

Table II. Primers used for qPCR in this study

Gene Name	Primer	Sequence (5′–3′)
Human-β-actin	h-β-actin-F	CCTTCCTGGGCATGGAGTCCTG
	h-β-actin-R	GGAGCAATGATCTTGATCTTC
Human-IFN-α	h-IFN-α-F	TTTCTCCTGCCTGAAGGACAG
	h-IFN-α-R	GCTCATGATTTCTGCTCTGACA
Human-IFN-β	h-IFN-β-F	ATGACCAACAAGTGTCTCCTCC
	h-IFN-β-R	GCTCATGGAAAGAGCTGTAGTG
Human-CCL5	h-CCL5-F	CCCCATATTCCTCGGACACC
	h-CCL5-R	GCTGTCCCTCTCTCTTTGGC
Human-CXCL10	h-CXCL10-F	TGCCATTCTGATTTGCTGCC
	h-CXCL10-R	TGATGGCCTTCGATTCTGGA
Human-Mx1	h-Mx1-F	CTCCGACACGAGTTCCACAA
	h-Mx1-R	GGCTCTTCCAGTGCCTTGAT
Human-ISG54	h-ISG54-F	AAGCACCTCAAAGGGCAAAAC
	h-ISG54-R	TCGGCCCATGTGATAGTAGAC
Human-ISG15	h-ISG15-F	CGCAGATCACCCAGAAGATCG
	h-ISG15-R	TTCGTCGCATTTGTCCACCA
Swine-IFN-β	sq-IFN-β-F	AGCACTGGCTGGAATGAAACCG
	sq-IFN-β-R	CTCCAGGTCATCCATCTGCCCA
Swine-IFN-α	sq-IFN-α-F	CTGCTGCCTGGAATGAGAGCC
	sq-IFN-α-R	TGACACAGGCTTCCAGGTCCC
Swine-β-actin	sq-β-actin-F	TGAGAACAGCTGCATCCACTT
	sq-β-actin-R	CGAAGGCAGCTCGGAGTT
Swine-ISG15	sq-ISG15-F	GGTGCAAAGCTTCAGAGACC
	sq-ISG15-R	GTCAGCCAGACCTCATAGGC
Swine-ISG56	sq-ISG56-F	TCAGAGGTGAGAAGGCTGGT
	sq-ISG56-R	GCTTCCTGCAAGTGTCCTTC
Swine-Mx1	sq-Mx1-F	AGCGCAGTGACACCAGCGAC
	sq-Mx1-R	GCCCGGTTCAGCCTGGGAAC
Swine-OAS2	sq-OAS2-F	CACAGCTCAGGGATTTCAGA
	sq-OAS2-R	TCCAACGACAGGGTTTGTAA
ASFV-B646L	ASFV-B646L-F	CTGCTCATGGTATCAATCTTATCGA
	ASFV-B646L-R	GATACCACAAGATCAGCCGT
	Probe	CCACGGGAGGAATACCAACCCAGTG

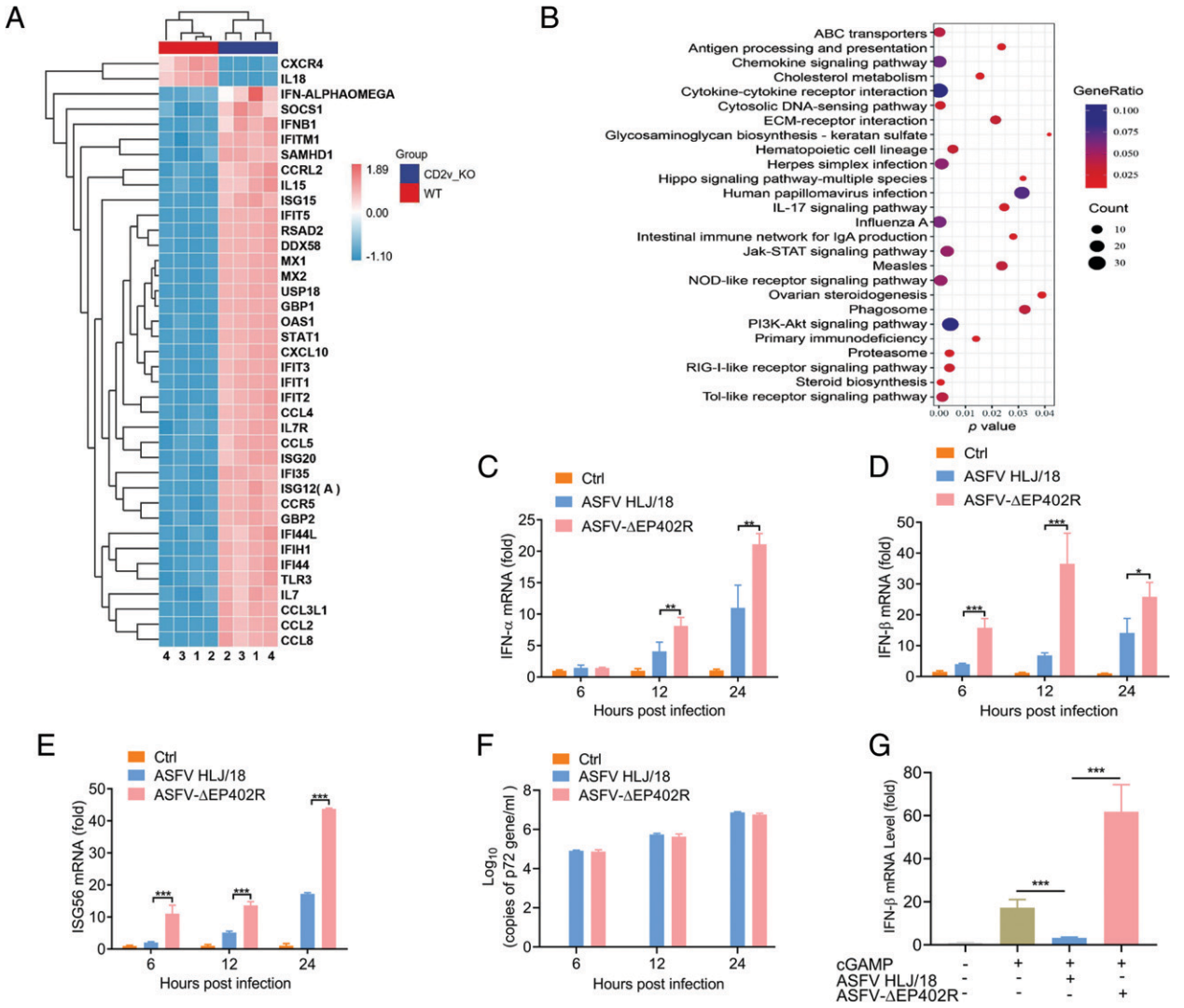

FIGURE 1. ASFV-ΔEP402R infection increases type I IFN production. (**A**) Heatmaps depicting changes in transcript levels of several inflammatory cytokines, IFNs, and ISGs between the ASFV HLJ/18– and ASFV-ΔEP402R–infected PAMs satisfied the threshold criterion for fold change (>1.5 or <0.67). (**B**) KEGG pathways associated with DEGs in the ASFV HLJ/18– and ASFV-ΔEP402R–infected PAMs. Dots represent term enrichment with color coding: red indicates high enrichment, and blue indicates low enrichment. The sizes of the dots represent the percentage of each row (Gene Ontology [GO] category). (**C**–**F**) PAMs were infected with ASFV HLJ/18 or ASFV-ΔEP402R at an MOI of 1 for 6, 12, and 24 h. The cells were collected to detect the mRNA levels of IFN-α (C), IFN-β (D), ISG56 (E), and ASFV genomic DNA (F) by qPCR. (**G**) PAMs were mock infected or infected with ASFV HLJ/18 or ASFV-ΔEP402R at an MOI of 1 for 12 h, and then the cells were treated with cGAMP for another 12 h. The mRNA level of IFN-β was then analyzed by qPCR. Data are representative of three independent experiments with three biological replicates (mean ± SD). $*p < 0.05$, $0.001 < **p < 0.01$, $***p < 0.001$ (one-way ANOVA).

The virulence of ASFV-ΔEP402R in SPF pigs

Twelve 8-wk-old SPF piglets were randomly divided into two groups (six piglets inoculated ASFV-ΔEP402R 10^3 HAD_{50}/piglet, six piglets inoculated ASFV HLJ/18 10^3 HAD_{50}/piglet). The piglets were monitored daily for clinical signs before feeding, including anorexia, lethargy, fever, and emaciation. The blood was collected at 0, 1, 4, 7, 10, 16 and 21 d postinoculation (dpi) for detecting virus load, and serum samples were collected at 0, 1, 4, and 7 dpi for detecting secretion of IFN-β, respectively.

ELISA

The concentrations of IFN-β protein levels in serum were measured by commercial ELISA kits specifically detecting IFN-β (Biorbyt, UK) according to the manufacturer's instructions.

Statistical analysis

All statistical analyses were performed using one-way ANOVA via the SPSS 16.0 software package (version 16.0; SPSS, Chicago, IL). Data were expressed as the mean ± SD. A p value <0.05 was considered statistically significant.

Results

ASFV-ΔEP402R infection enhances type I IFN production

Previous studies showed that the inhibition of IFN production and its downstream signaling is related to the pathogenicity of ASFV (30). Recently, EP402R was reported to be involved in ASFV pathogenicity (31); however, the effect of EP402R on type I IFN production is not fully understood. To study the effect of EP402R on innate immune responses, we generated a recombinant ASFV-ΔEP402R by deletion of EP402R gene using homologous recombination. Full-length genomic comparison between ASFV-ΔEP402R and it parental ASFV HLJ/18 demonstrated a deletion of 1083 nt and the insertion of an 801-nt construct corresponding to the p72-GFP cassette sequence. GFP was expressed successfully under the control of the B646L gene promoter. The PBMCs infected with ASFV-ΔEP402R lost hemadsorption property (Supplemental Fig. 1A). ASFV-ΔEP402R displayed a growth kinetic similar to that of its parental virus ASFV HLJ/18 (Supplemental Fig. 1B), suggesting that

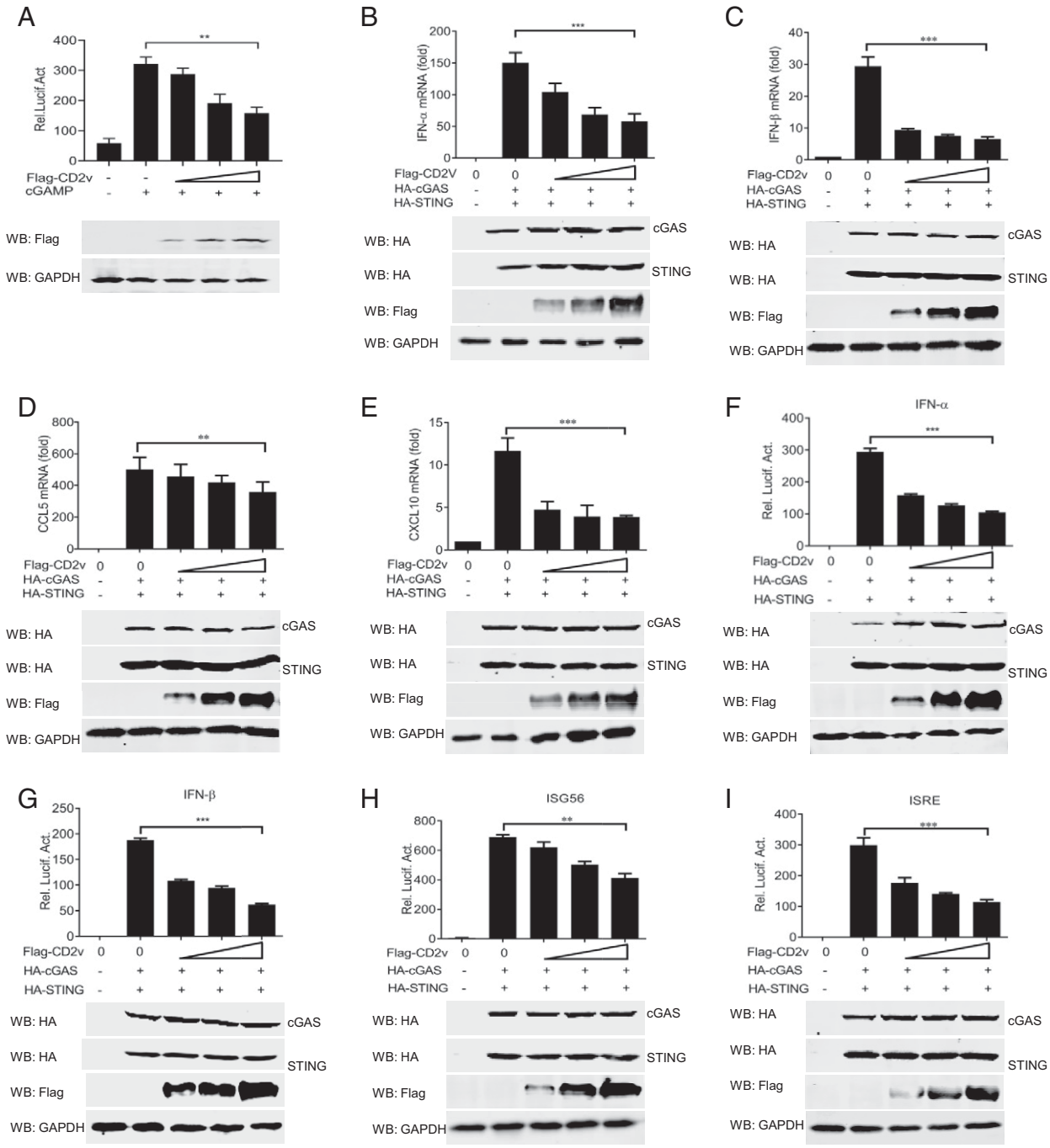

FIGURE 2. ASFV CD2v inhibits type I IFN production induced by cGAS-STING. (**A**) HEK293T-STING cells were transfected with a Luciferase reporter and a Renilla-TK reporter, together with increasing amounts (0, 100, 200, and 400 ng) of a plasmid expressing Flag-CD2v for 12 h, and then the cells were treated with cGAMP for another 12 h. Luciferase activities were then analyzed. The expressions of all proteins were analyzed by Western blotting with GAPDH as an internal control. (**B**–**E**) HEK293T cells were transfected with two plasmids expressing HA-cGAS and HA-STING, respectively, together with increasing amounts (0, 100, 200, and 400 ng) of a plasmid expressing Flag-CD2v for 24 h. The mRNA levels of IFN-α (B), IFN-β (C), CCL5 (D), and CXCL10 (E) in the HEK293T cells were analyzed by qPCR. The expressions of all proteins were analyzed by Western blotting with GAPDH as an internal control. (**F**–**I**) HEK293T cells were transfected with an IFN-α– (F), IFN-β– (G), ISG56- (H), or ISRE-Luc (I) reporter and a Renilla-TK reporter, two plasmids expressing HA-cGAS and HA-STING, respectively, together with increasing amounts (0, 100, 200, and 400 ng) of a plasmid expressing Flag-CD2v for 24 h. Luciferase activities were then analyzed. The expressions of all proteins were analyzed by Western blotting with GAPDH as an internal control. Data are representative of three independent experiments with three biological replicates (mean ± SD). $0.001 < **p < 0.01$, $***p < 0.001$ (one-way ANOVA).

deletion of EP402R gene in ASFV HLJ/18 does not significantly affect the ability of the virus replication in PAMs (Tables I, II).

To compare the differences of gene expression during ASFV HLJ/18 and ASFV-ΔEP402R infection, we investigated DEGs in PAMs at 24 h postinfection (hpi) with ASFV HLJ/18 and ASFV-ΔEP402R using the RNA sequencing (RNA-seq) technique. Compared with ASFV HLJ/18, a total of 3046 DEGs (with fold change > 2, $p < 0.05$) were detected in ASFV-ΔEP402R–infected PAMs (Supplemental Fig. 2A). Interestingly, deletion of EP402R from ASFV induced higher type I IFN and ISG production than wild

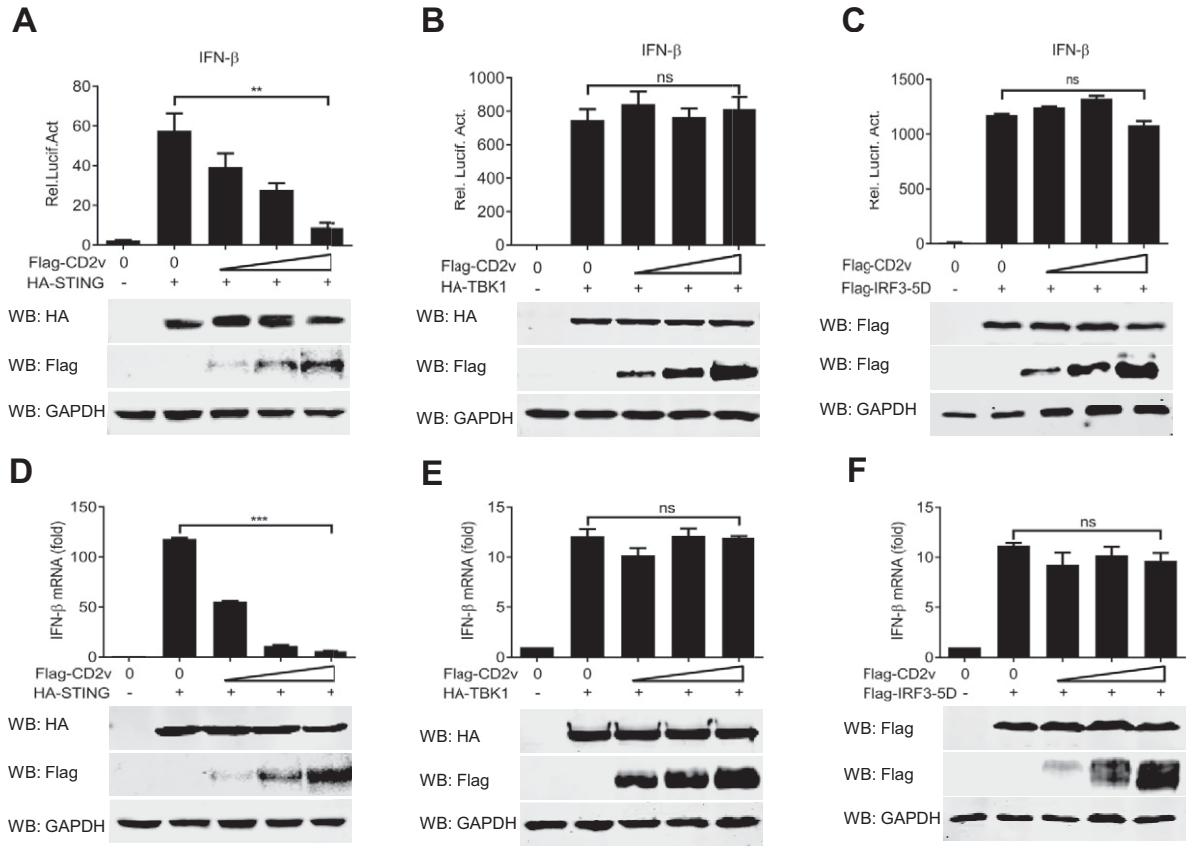

FIGURE 3. ASFV CD2v inhibits type I IFN production by targeting STING. (**A**–**C**) HEK293T cells were transfected with an IFN-β Luc reporter and a Renilla-TK reporter, a plasmid expressing HA-STING (A), HA-TBK1 (B), or HA-IRF3-5D (C), together with an empty vector or different amounts (0, 100, 200, and 400 ng) of a plasmid expressing Flag-CD2v for 24 h; the cells were collected for detection of the luciferase activity. The expression levels of HA-STING, HA-TBK1, HA-IRF3-5D, Flag-CD2v, and GAPDH were detected by Western blotting. (**D**–**F**) HEK293T cells were transfected with a plasmid expressing HA-STING (D), HA-TBK1 (E), or HA-IRF3-5D (F), together with an empty vector or increasing amounts of a plasmid expressing Flag-CD2v. The cells were collected at 24 hpt, and the mRNA levels of IFN-β were analyzed by qPCR. The expressions of HA-STING, HA-TBK1, HA-IRF3-5D, Flag-CD2v, and GAPDH were detected by Western blotting. Data are representative of three independent experiments with three biological replicates (mean ± SD). $^{ns}p > 0.05$, $0.001 < **p < 0.01$, $***p < 0.001$ (one-way ANOVA). ns, not significant.

type (WT) ASFV (Fig. 1A). To identify the biological pathways of DEGs, we annotated the assembled unigenes against the KEGG database and assigned them to 87 different KEGG pathways, including several IFN-related signaling pathways, such as TLR, retinoic acid-inducible gene 1–like receptor, cytosolic DNA-sensing, and JAK-STAT signaling pathways (Fig. 1B).

To confirm that ASFV-ΔEP402R infection induces more type I IFN production and ISG expression in PAMs than those infected with ASFV HLJ/18, we infected PAMs with ASFV-HLJ/18 or ASFV-ΔEP402R at an MOI of 1 for 6, 12, and 24 h, respectively, and then the cells were collected to detect the mRNA levels of IFN-α, IFN-β, ISG56, and ASFV genomic DNA copy number using qPCR. As shown in Fig. 1C–E, ASFV-ΔEP402R infection induced higher mRNA levels of IFN-α, IFN-β, and ISG56 than ASFV HLJ/18 infection. The genomic copy numbers of ASFV-ΔEP402R and ASFV HLJ/18 were almost the same at 6, 12, and 24 hpi (Fig. 1F). To further detect the role of ASFV-ΔEP402R on IFN-β production, we infected PAMs with ASFV HLJ/18 or ASFV-ΔEP402R and then treated them with cGAMP. The results showed that ASFV HLJ/18 inhibited the mRNA level of IFN-β, but not ASFV-ΔEP402R (Fig. 1G, Table II). Taken together, these results indicate that EP402R-encoded protein (CD2v) of ASFV HLJ/18 may negatively regulate type I IFN production.

To analyze whether CD2v of other ASFV strains plays a similar role in inhibiting type I IFN and ISG production during infection, we examined multiple-sequence alignment among 12 EP402R genes from genotype I and genotype II ASFV using BLAST (https://blast.ncbi.nlm.nih.gov/Blast.cgi). The data showed that the amino acid sequences of CD2v from genotype II ASFV, including ASFV HLJ/18, were 100% homologous, indicating that CD2v is highly conserved in genotype II ASFV. However, it had greater variability between ASFV-HLJ/18 CD2v and CD2v from genotype I ASFV (Supplemental Fig. 2B). Therefore, we speculated that it is universal for CD2v from genotype II ASFV in inhibiting type I IFN and ISG production.

ASFV CD2v suppresses the cGAS-STING signaling pathway

On ASFV infection, cGAS can sense cytosolic viral DNA and trigger type I IFN–mediated antiviral immune responses (32, 33). To further identify the inhibitory effect of CD2v on type I IFN production, we transfected HEK293T-STING cells with stable expressing STING with IFN-β luciferase and TK, together with different doses of a plasmid expressing CD2v, and then treated with cGAMP or poly(I:C); the results showed that CD2v inhibited cGAMP-induced, but not poly(I:C)–induced, IFN-β promoter activity in a dose-dependent manner (Fig. 2A, Supplemental Fig. 3A). To verify the results, we transfected HEK293T cells with plasmids expressing cGAS and STING, together with increasing doses of a plasmid expressing Flag-CD2v, and then collected the cells for detection of the mRNA levels of IFN-α, IFN-β, CXCL10, and CCL5 by qPCR. The results showed that ectopically expressed CD2v

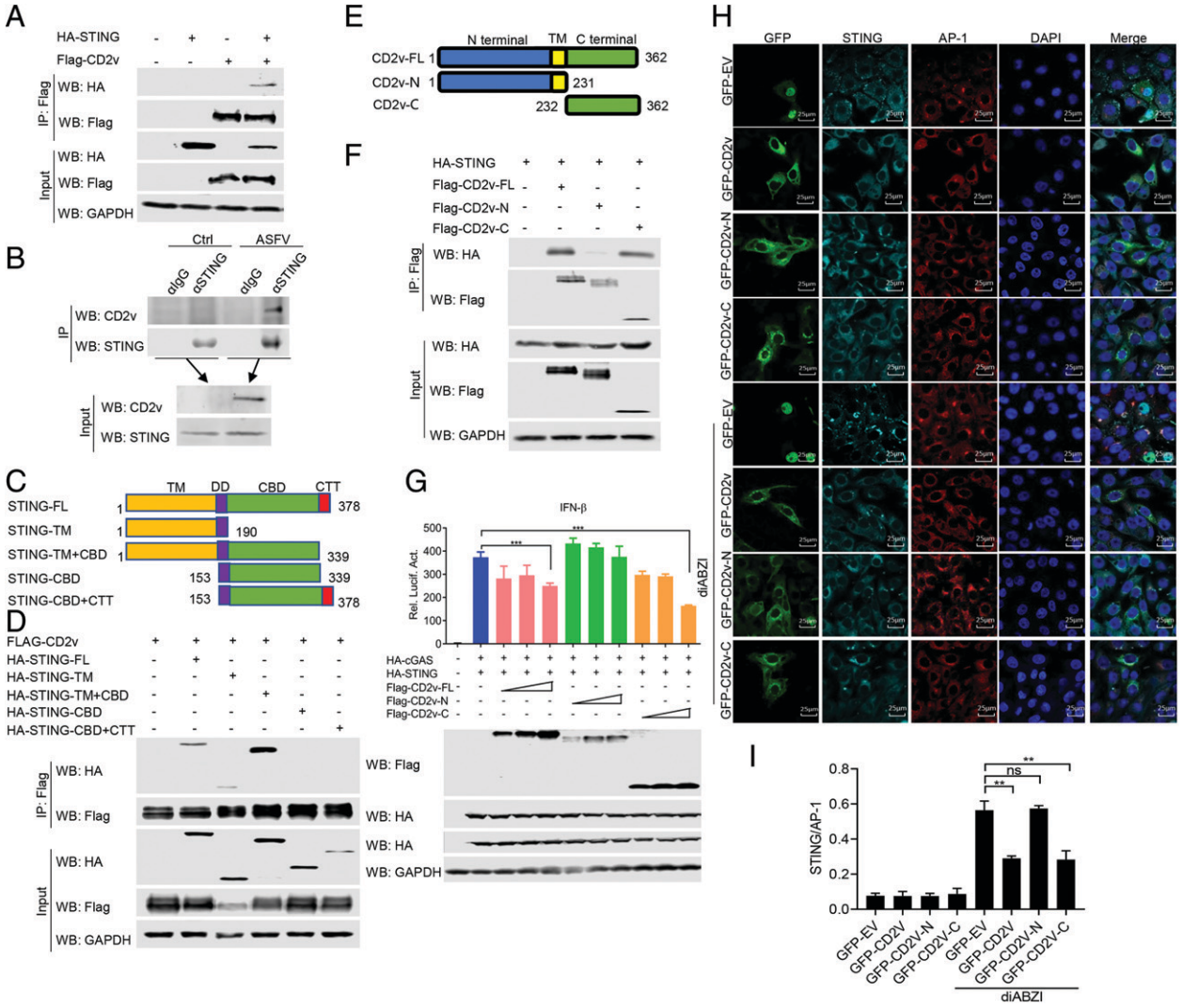

FIGURE 4. ASFV CD2v interacts with STING. (**A**) Co-IP analysis of the interaction between CD2v and STING in HEK293T cells. (**B**) Co-IP analysis of the interaction between endogenous CD2v and STING in PAMs that were mock infected or infected with ASFV. (**C**) Schematic of full-length STING and its deleted mutants. (**D**) HEK293T cells were transfected with a plasmid expressing Flag-CD2v, along with plasmids expressing HA-STING-WT, HA-STING-TM, HA-STING-TM+CBD, HA-STING-CBD, and HA-STING-CBD+cytoplasmic-terminal tail, respectively. The cells were collected at 24 hpi, and the interaction of STING and CD2v or its deleted mutants were analyzed by Co-IP and Western blotting. (**E**) Schematic of full-length CD2v and its deleted mutants. (**F**) HEK293T cells were transfected with a plasmid expressing HA-STING alone or together with plasmids expressing Flag-CD2v-WT and its deleted mutants, including Flag-CD2v-ΔN, Flag-CD2v-ΔC, and Flag-CD2v-C, respectively. The interaction of STING and CD2v and its deleted mutants were analyzed by Co-IP and Western blotting. (**G**) HEK293T cells were transfected with an IFN-β Luc reporter and a Renilla-TK reporter, along with plasmids expressing HA-cGAS and HA-STING, along with increasing amounts of a plasmid expressing Flag-CD2v or its deleted mutants. The cells were collected to detect the luciferase activity or test the expression of these indicated proteins by Western blotting. (**H**) The subcellular localization of CD2v and STING in MA104 cells expressing GFP or GFP-CD2v and then mock treated or treated with diABZI. Twelve hours later, the localization of CD2v (green) and STING (cyan) was detected by immunofluorescence microscopy. Scale bars, 5 μm. (**I**) The fluorescence intensity of the images was analyzed using the Zeiss processing system. Data are representative of three independent experiments with three biological replicates (mean ± SD). $0.001 < **p < 0.01$, $***p < 0.001$ (one-way ANOVA). ns, not significant.

significantly decreased the mRNA levels of IFN-α, IFN-β, CCL5, and CXCL10 induced by cGAS and STING (Fig. 2B–E). In agreement with the results, CD2v also inhibited IFN-α, IFN-β, ISG56, and ISRE promoter activities induced by cGAS and STING (Fig. 2F–I), whereas O61R had no effect on IFN-β promoter activity (Supplemental Fig. 3B). Taken together, these results indicate that ASFV CD2v can significantly inhibit cGAS-STING–induced type I IFN production.

ASFV CD2v inhibits type I IFN production by targeting STING

To elucidate the underlying molecular mechanism by which ASFV CD2v negatively regulates the cGAS-STING signaling pathway, we first assessed the effect of ASFV CD2v on IFN-β promoter activation induced by the key molecules in the cGAS-STING signaling pathway in HEK293T cells. As shown in Fig. 3A–C, overexpressed ASFV CD2v significantly reduced the IFN-β promoter activity induced by STING in a dose-dependent manner, but not by TBK1 and IRF3-5D, a constitutively active IRF3 variant (34). Consistent with these results, the mRNA levels of IFN-β were also attenuated by ASFV CD2v in the HEK293T cells induced by STING (Fig. 3D). However, the mRNA levels of IFN-β mediated by TBK1 (Fig. 3E) and IRF3-5D (Fig. 3F) were not impaired by ASFV CD2v. These results suggest that ASFV CD2v may target STING to inhibit type I IFN production.

ASFV CD2v inhibits STING translocation to Golgi apparatus through interacting with the TM of STING

To detect the interaction between CD2v and key molecules involved in the cGAS-STING pathway, we transfected HEK293T cells with

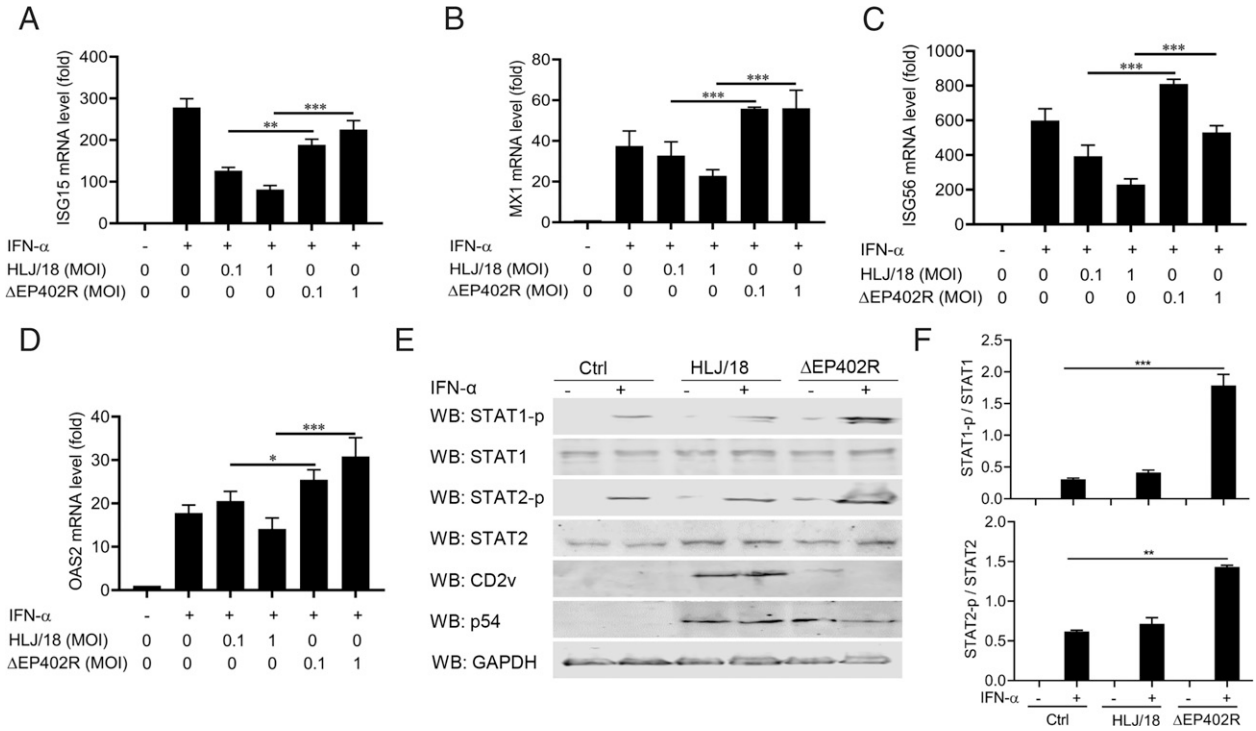

FIGURE 5. Deletion of EP402R from ASFV HLJ/18 promotes JAK-STAT activation in IFN signaling. (**A**–**D**) PAMs were infected with 0.1 or 1 MOI of ASFV HLJ/18 or ASFV-ΔEP402R, and then the cells were treated with IFN-α. The mRNA levels of ISG15 (A), MX1 (B), ISG56 (C), and OAS2 (D) were detected by qPCR. (**E**) PAMs were mock infected or infected with 1 MOI of ASFV HLJ/18 or ASFV-ΔEP402R, and then the cells were mock treated or treated with IFN-α. The expressions of STAT1, STAT1-p, STAT2, STAT2-p, CD2v, p54, and GAPDH were detected by Western blotting. (**F**) The ratio of the intensity value of the STAT1-p/STAT1 and STAT2-p/STAT2 immunoblotting result from (E) was quantified by ImageJ. Data are representative of three independent experiments with three biological replicates (mean ± SD). $*p < 0.05$, $0.001 < **p < 0.01$, $***p < 0.001$ (one-way ANOVA).

a plasmid expressing CD2v alone or together with a plasmid expressing cGAS, STING, TBK1, or IRF3. Co-IP was performed at 24 h post transfection, and the results showed that CD2v interacted with STING, but not with other proteins (Supplemental Fig. 4A, 4B). The interaction between overexpressed CD2v and STING was further confirmed in HEK293T cells (Fig. 4A). Consistent with these results, endogenous CD2v also interacted with endogenous STING in PAMs during ASFV infection (Fig. 4B). STING is an ER membrane protein that contains four TMs followed by a cytoplasmic ligand-binding and signaling domain. To map which domain of STING is required for the interaction with CD2v, we constructed four different plasmids encoding Flag-tagged STING mutants (STING-TM, STING-TM+CDN-binding domain (CBD), STING-CBD, STING-ΔTM) (Fig. 4C, Table I). The results of Co-IP showed that CD2v interacted with STING-TM and STING-TM+CBD, but not STING-CBD or STING-ΔTM, suggesting that the TM domain of STING is required for the interaction between CD2v and STING (Fig. 4D). On ASFV infection, CD2v is cleaved into an N-terminal fragment with glycosylation and a C-terminal fragment without glycosylation. To map which fragment of CD2v was necessary to interact with STING, we constructed three deleted mutants of CD2v (CD2v-N, CD2v-ΔN, CD2v-C) (Fig. 4E). The results revealed that the C terminus of CD2v was indispensable for interacting with STING (Fig. 4F). Consistent with these results, the C terminus of CD2v inhibited IFN-β promoter activity induced by cGAS-STING (Fig. 4G).

It has been reported that the translocation of STING from ER to Golgi apparatus is necessary for STING activation (13, 35), and the *trans*-Golgi network is impaired in ASFV-infected cells (36). To explore whether CD2v affects the translocation of STING in the Golgi apparatus, we treated the cells with diamidobenzimidazole (diABZI), a STING agonist that belongs to a family of small-molecule amidobenzimidazoles (ABZIs) (37), and we detected the localization of CD2v and STING by confocal microscopy experiment. As shown in Fig. 4H and 4I, STING colocated with activator protein 1, which is a Golgi apparatus marker on diABZI stimulation. However, an overexpressed full-length and C-terminal fragment, but not N-terminal fragment, of CD2v disrupted the location of STING on Golgi apparatus on diABZI stimulation. These results suggest that the C terminus of CD2v can inhibit the translocation of STING to the Golgi apparatus.

ASFV CD2v inhibits ISG expression

The results of RNA-seq showed that ASFV-ΔEP402R infection enhanced the expression of ISGs, including ISG15, Mx2, and several IFN-induced protein with tetratricopeptide repeats molecules. To confirm these results, we infected PAMs with ASFV HLJ/18 or ASFV-ΔEP402R and then treated them with IFN-α; the results showed that ASFV-ΔEP402R infection induced higher mRNA levels of ISG56, ISG15, Mx1, and OAS2 with IFN-α treatment than that of ASFV HLJ/18 infection (Fig. 5A–D). Consistent with these results, the phosphorylation of STAT1 and STAT2 on IFN-α stimulation was blocked by ASFV HLJ/18, but not ASFV-ΔEP402R, infection (Fig. 5E, 5F). The earlier results showed that CD2v may negatively regulate the type I IFN signaling pathway. To verify the speculation, an increasing amount of a plasmid expressing CD2v, along with pRL-TK, we transfected ISRE, ISG56, and ISG54 reporter into HEK293T cells, and then the cells were treated with IFN-α for 12 h. The results showed that CD2v inhibited the activities of ISRE, ISG56, and ISG54 promoter induced by IFN-α in a dose-dependent manner (Fig. 6A–C), whereas O61R had no effect on the activity of ISRE promoter induced by IFN-α (Fig. 6D). Consistent with these

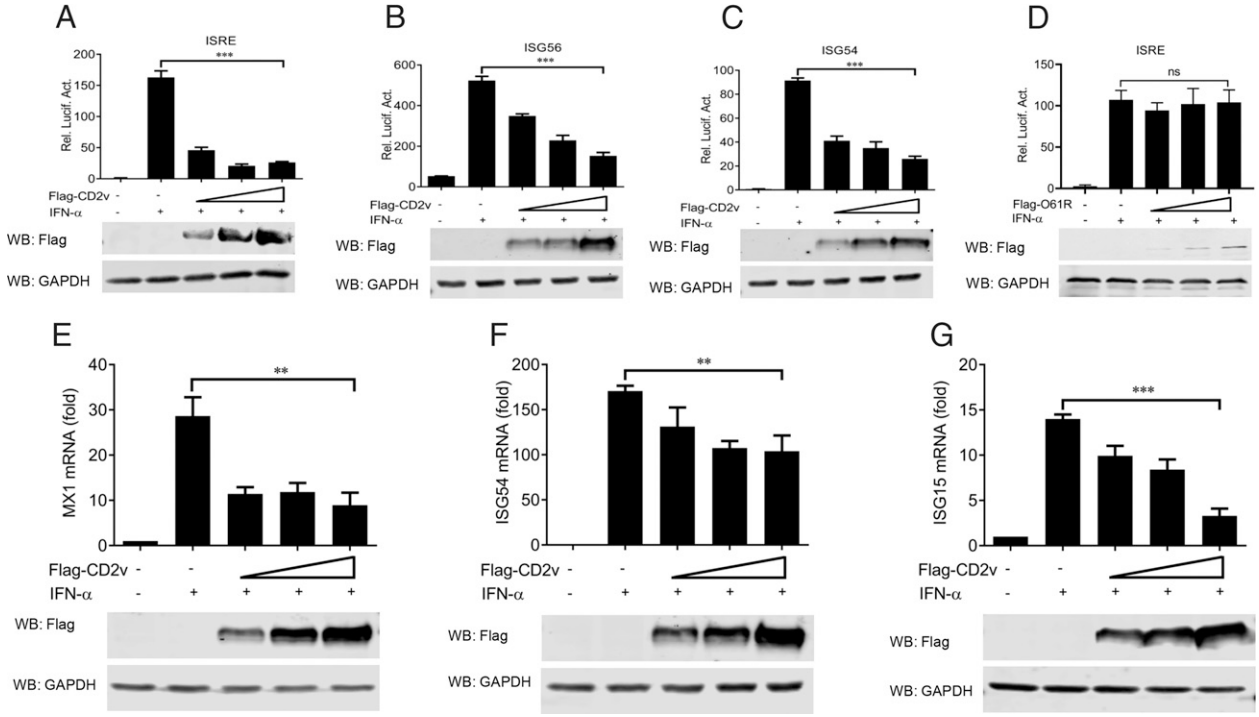

FIGURE 6. ASFV CD2v inhibits JAK-STAT activity in IFN signaling. (**A**–**D**) HEK293T cells were transfected with an ISRE- (A and D), ISG56- (B), or ISG54-Luc reporter (C) and a Renilla-TK reporter, together with different amounts (0, 100, 200, and 400 ng) of a plasmid expressing Flag-CD2v (A–C) or Flag-O61R (D). At 24 h post transfection, the cells were treated with IFN-α. Luciferase activities were then analyzed. The expressions of all proteins were analyzed by Western blotting with GAPDH as an internal control. (**E**–**G**) HEK293T cells were transfected with different amounts (0, 100, 200, and 400 ng) of a plasmid expressing Flag-CD2v for 24 h, and then the cells were treated with IFN-α for 12 h. The mRNA levels of Mx1 (E), ISG54 (F), and ISG15 (G) in the HEK293T cells were analyzed by qPCR. The expressions of all proteins were analyzed by Western blotting with GAPDH as an internal control. Data are representative of three independent experiments with three biological replicates (mean ± SD). $^{ns}p > 0.05$, $0.001 < **p < 0.01$, $***p < 0.001$ (one-way ANOVA). ns, not significant.

results, CD2v also inhibited the mRNA level of Mx1, ISG54, and ISG15 induced by IFN-α in a dose-dependent manner (Fig. 6E–G).

ASFV CD2v disrupts the interactions of IFNAR1-TYK2 and IFNAR2-JAK1

To clarify the role of ASFV CD2v on ISG production, we examined the interaction between CD2v and IFNAR1, IFNAR2, JAK1, TYK2, STAT1, STAT2, and IRF9. The results showed that CD2v interacted with IFNAR1 and IFNAR2, but not with other proteins in the JAK-STAT signaling pathway (Supplemental Fig. 4C). To confirm these results, we cotransfected HEK293T cells with a plasmid expressing GFP-CD2v together with a plasmid expressing Flag-IFNAR1 or Flag-IFNAR2. The results showed that CD2v was coimmunoprecipitated with both IFNAR1 and IFNAR2 (Fig. 7A, 7B). Consistent with these results, CD2v interacted with endogenous IFNAR1 and IFNAR2 on ASFV infection (Fig. 7C). It has been reported that once type I IFNs bind to IFNAR1 and IFNAR2, IFNAR1 and IFNAR2 recruit TYK2 and JAK1, respectively. We found that overexpressed CD2v disrupts the interaction of IFNAR1-TYK2 (Fig. 7D) and IFNAR2-JAK1 (Fig. 7E). In addition, overexpressed CD2v also inhibited the phosphorylation of STAT1 and STAT2 and the following translocation of STAT1 and STAT2 into the nucleus on IFN-α stimulation (Fig. 7F–H). All these results indicate that CD2v inhibits the recruitment of TYK2 and JAK1 by IFNAR1 and IFNAR2 through interacting with IFNAR1 and IFNAR2, which leads to reduced phosphorylation and translocation of STAT1 and STAT2.

ASFV-ΔEP402R has lower pathogenicity and induces more IFN-β in pigs

To detect the role of EP402R gene in pathogenicity of ASFV HLJ/18, we challenged SPF pigs with ASFV HLJ/18 or ASFV-ΔEP402R. Body temperature was detected every day, and survival ratio was monitored postinoculation. As shown in Fig. 8A, the pigs in the ASFV HLJ/18–inoculated group developed fever at 3 dpi, and the pigs in ASFV-ΔEP402R–inoculated group developed fever at 5 dpi. We evaluated the clinical scores of the infected pigs, and the results showed that the clinical scores of the pigs infected with ASFV-ΔEP402R were significantly lower than those with ASFV HLJ/18 (Fig. 8B). All of the pigs challenged with ASFV HLJ/18 died within 10 dpi, whereas the survival rate in the ASFV-ΔEP402R–challenged group was 40% (Fig. 8C). Blood samples were collected at 1, 4, 7, 10, 16, and 21 dpi for viral DNA quantification by qPCR. As shown in Fig. 8D, the average viral DNA copies in blood from the ASFV-ΔEP402R–inoculated group were 3–4 logs lower at 4, 7, and 10 dpi than that in the ASFV HLJ/18–inoculated group.

To evaluate the antiviral response of pigs to ASFV challenge, we monitored the IFN-β protein levels in peripheral blood at 0, 1, 4, and 7 dpi using ELISA. The results showed that the IFN-β levels in peripheral blood from the ASFV HLJ/18– and ASFV-ΔEP402R–inoculated pigs were almost the same at 4 dpi, and the IFN-β levels from ASFV-ΔEP402R–inoculated pigs were significantly higher than that from ASFV HLJ/18–inoculated pigs at 7 dpi (Fig. 8E).

In summary, on ASFV infection, CD2v interacts with STING to attenuate its localization on Golgi, resulting in inhibition of type I IFNs production. In addition, CD2v interacts with IFNAR1 and IFNAR2 to destruct the interactions between IFNAR1 and TYK2 and IFNAR2 and JAK1 to inhibit ISG expression (Fig. 9). Compared with its parental ASFV HLJ/18, ASFV-ΔEP402R infection enhances the production of type I IFN and ISG expression in PAMs and reduces the pathogenicity of ASFV HLJ/18 with enhanced type I IFN production in the ASFV-ΔEP402R–infected pigs.

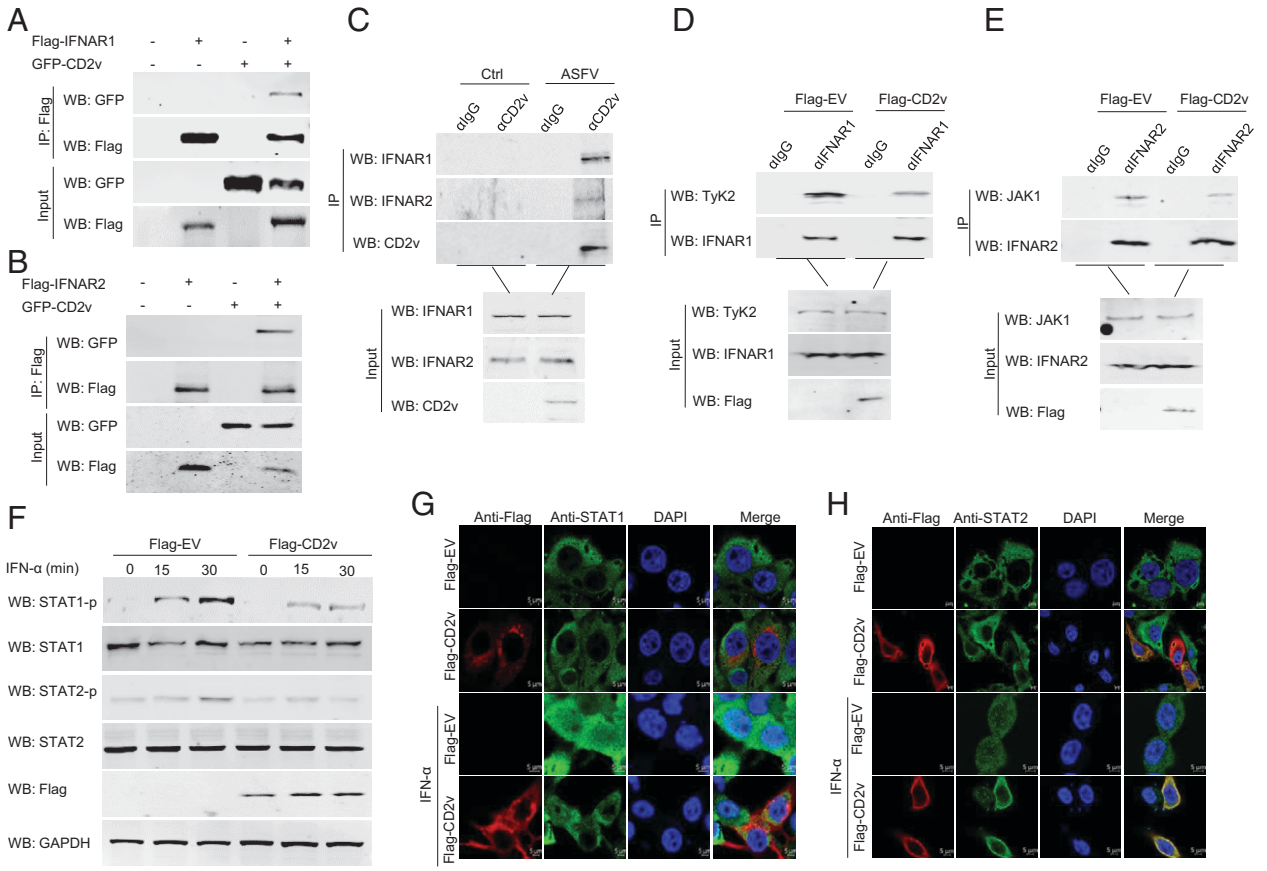

FIGURE 7. ASFV CD2v inhibits the interaction of IFNAR1-TYK2 and IFNAR2-JAK1. (**A** and **B**) HEK293T cells were transfected with a plasmid expressing GFP-CD2v or an empty vector, along with a plasmid expressing Flag-IFNAR1 or Flag-IFNAR2. The interactions between CD2v and IFNAR1 and CD2v and IFNAR2 were analyzed by Co-IP and Western blotting. (**C**) PAMs were mock infected or infected with ASFV (MOI = 1) for 24 h, and then the cells were collected for Co-IP analysis of the interaction between CD2v and endogenous IFNAR1 and IFNAR2. (**D** and **E**) MA104 cells were transfected with a plasmid expressing GFP-CD2v or an empty vector. The interaction between IFNAR1 and TYK2 or between IFNAR2 and JAK1 was analyzed by Co-IP and Western blotting. (**F**) MA104 cells were transfected with an empty vector or a plasmid expressing Flag-CD2v. The cells were treated with IFN-α for 0, 15, and 30 min, and then the expressions of STAT1, STAT1-p, STAT2, STAT2-p, CD2v, and GAPDH were detected by Western blotting. (**G** and **H**) MA104 cells were transfected with a plasmid expressing an empty vector or a plasmid expressing Flag-CD2v. The cells were treated with IFN-α for 6 h, and then the localization of CD2v (red) and STAT1 (green) (G) or STAT2 (green) (H) was detected by immunofluorescence microscopy. Scale bars, 5 μm. Data are representative of three independent experiments with three biological replicates.

Discussion

It has been reported that deletion of EP402R gene from several ASFV strains attenuated their pathogenicity (25, 31, 38, 39). In the study, the transcriptome of PAMs infected with ASFV-ΔEP402R and ASFV HLJ/18 was analyzed using RNA-seq. The KEGG analysis results showed that the innate immune process was differently regulated in PAMs on ASFV HLJ/18 and ASFV-ΔEP402R infection. Compared with its parental ASFV HLJ/18, ASFV-ΔEP402R infection induced higher levels of type I IFN production and ISG expression in PAMs. Subsequently, we confirmed that overexpressed ASFV HLJ/18 CD2v inhibits type I IFN production and ISG expression and suppresses cGAS-STING and IFN signaling pathways. Interestingly, we also found that deletion of EP402R gene from ASFV HLJ/18 increased the mRNA and protein level of IFN-β and reduced the pathogenicity of ASFV in vivo, revealing the underlying mechanisms by which ASFV EP402R antagonizes IFN production and ISG expression, which is closely related to ASFV pathogenicity.

The cGAS-STING signaling pathway can be activated to execute antiviral function on DNA virus infection (40). Previous studies demonstrate that DNA viruses have evolved various mechanisms to antagonize the cGAS-STING–induced antiviral innate immune responses for their efficient infection and avoiding being cleared (41). ASFV is a large, dsDNA virus, and it can replicate successfully in macrophages and monocytes (42). To replicate in these immune cells, ASFV has developed counteracting measures against host antiviral innate immune responses (43), including NF-κB, cGAS-STING, and IFN signaling pathways. Several ASFV proteins have been identified as inhibitors in the NF-κB signaling pathway. For example, the MGF360-12L inhibits type I IFN production by inhibiting the NF-κB signaling pathway (7). As a functional viral TLR3 homolog, the pI329L suppresses type I IFN production by targeting the TRIF (44, 45). In addition, several ASFV proteins were observed to modulate different steps in the cGAS-STING signaling pathway. For example, pMGF505-7R/pA528R inhibits the cGAS-STING signaling pathway by degrading STING and inhibiting the translocation of IRF3-5D into the nucleus (9, 46). ASFV pE120R suppresses the phosphorylation of IRF3 and the production of type I IFN by binding to IRF3 and blocking the recruitment of IRF3 to TBK1 (47). ASFV pI215L recruits RNF138 to degrade RNF128 to inhibit K63 phosphorylation of TBK1 mediated by RNF128 (33). The ASFV pA276R inhibits IFN-β induction via both the TLR3 and the cytosolic pathways by targeting IRF3, but not IRF7 or NF-κB (5).

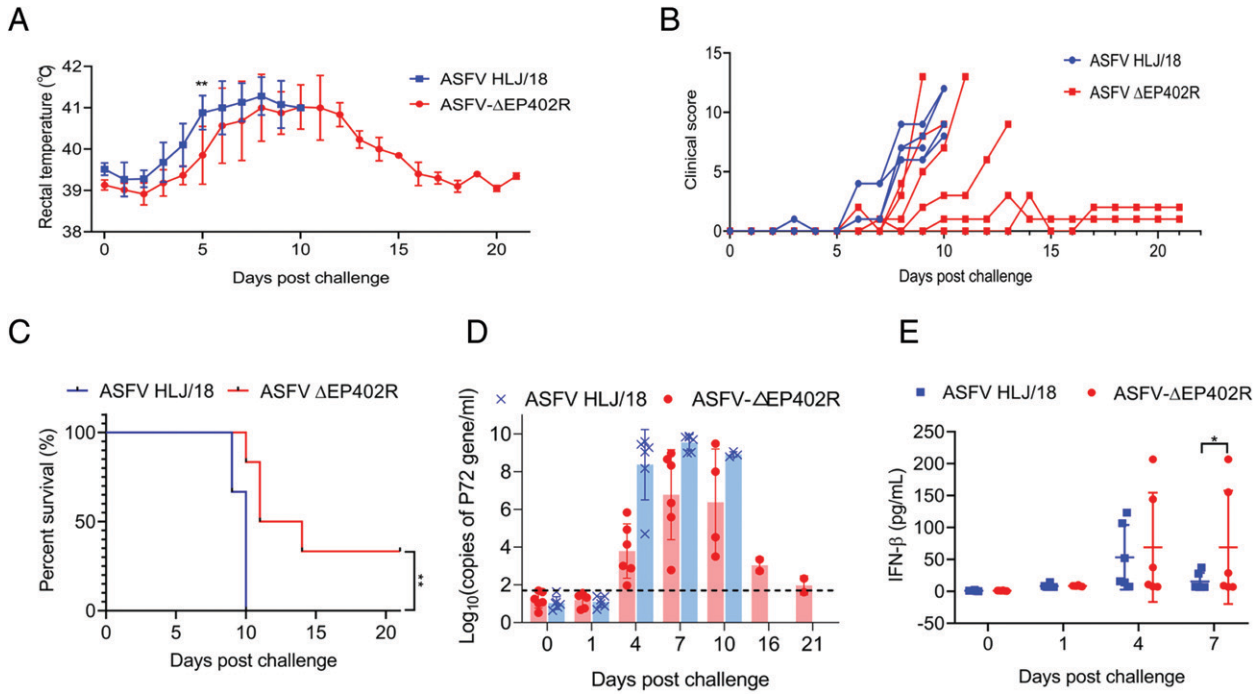

FIGURE 8. ASFV-ΔEP402R infection increases IFN production, resulting in reduction of the pathogenicity of ASFV. (**A**–**C**) Body temperatures (A), clinical score (B), and survival rates (C) of pigs i.m. infected with 10^3 HAD_{50} of either ASFV-ΔEP402R or parental ASFV HLJ/18. (**D**) qPCR analysis of ASFV genomic DNA copy number in blood samples obtained from pigs at 0, 1, 4, 7, 10, 16, and 21 d after infection with 10^3 HAD_{50} of either ASFV-ΔEP402R or its parental ASFV HLJ/18. (**E**) Detection of IFN-β in blood samples obtained from pigs at 0, 1, 4, and 7 d after infection with either ASFV HLJ/18 or ASFV-ΔEP402R using ELISA. $^{ns}p > 0.05$, $*p < 0.05$, $0.001 < **p < 0.01$ (two-way ANOVA). ns, not significant.

Furthermore, several ASFV proteins were found to suppress the IFN signaling pathway. The pMGF505-7R/pA528R is able to negatively regulate the IFN signaling pathway (48). However, several members of MGF360 and MGF505/530 were also reported to inhibit the induction of type I IFNs with unknown mechanisms (10). In our previous study, we screened the candidate ASFV-encoded proteins involved in inhibiting type I IFN production via antagonizing the cGAS-STING signaling pathway, and CD2v was identified as one of the inhibitors. In this study, we found that overexpressed CD2v inhibited the activities of the IFN-β, ISRE, NF-κB, and ISG56 promoters and the mRNA levels of the IFN-β and ISG56 induced by cGAS-STING. Further study showed that ectopic expression of CD2v significantly inhibited STING-mediated, but not TBK1- and IRF3/5D-mediated, activation of the IFN-β promoter.

ASFV CD2v is an ASFV-encoded glycoprotein containing a signal peptide, a TM, and two Ig-like domains. Previous studies have described CD2v as an immunomodulatory factor in inhibition of mitogen-induced proliferation of lymphocytes in vitro (21). On ASFV infection, CD2v is cleaved into the N-terminal fragment with glycosylation and C-terminal fragments without glycosylation (20). Both of the forms coexist with the full-length protein in ASFV-infected cells. However, only the band of full length of ~89 kDa was detected in CD2v-overexpressed or ASFV-infected cells. The reason for these results might be because of the low sensitivity of the CD2v Ab, or the mAb we used only specifically recognizes epitopes of full-length CD2v. In this study, we found that the C-terminal fragment is required for the inhibition activity of the IFN-β promoter induced by cGAS-STING, whereas the C-terminal fragment is necessary for the interaction between CD2v and STING, suggesting that the glycosylation of CD2v may be independent of its function in cGAS-STING signaling. However, it was reported that CD2v of the ASFV Congo K-49 strain activates NF-κB, which induces IFN signaling and apoptosis in swine lymphocytes/macrophages. We compared the sequence of CD2v of Congo K-49 and HLJ/18 and found that the sequence homology is only 50%. CD2v of HLJ/18 has 489 aa, and CD2v of Congo K-49 has only 459 aa (26). Therefore, it is not difficult to understand that CD2v of different strains have different functions on type I IFN production.

Type I IFNs bind onto IFNAR1 and IFNAR2 on the cell membrane, and then the receptors recruit TYK2 and JAK1 to active JAK-STAT in the IFN signaling pathway, resulting in ISG expression. It has been reported that ASFV MGF360-9L interacts with STAT1 and STAT2 and degrades STAT1 and STAT2 through apoptosis and ubiquitin-proteasome pathways to inhibit ISG expression (49). In this study, we found that CD2v competes with TYK2 and JAK1 to interact with IFNAR1 and IFNAR2, which leads to inhibited ISG production. These results reveal a new underlying mechanism by which ASFV EP402R antagonizes type I IFN production.

In summary, we report that ASFV CD2v regulates the pathogenicity of ASFV HLJ/18 by inhibiting both type I IFN production and the IFN signaling pathway. Mechanistically, CD2v not only inhibits STING localization on Golgi apparatus through interacting with the TM domain of STING but also inhibits ISG production by disrupting the interactions of IFNAR1-TYK2 and IFNAR2-JAK1.

Acknowledgments

We thank Prof. Dongming Zhao for the ASFV HLJ/18 strain.

Disclosures

The authors have no financial conflicts of interest.

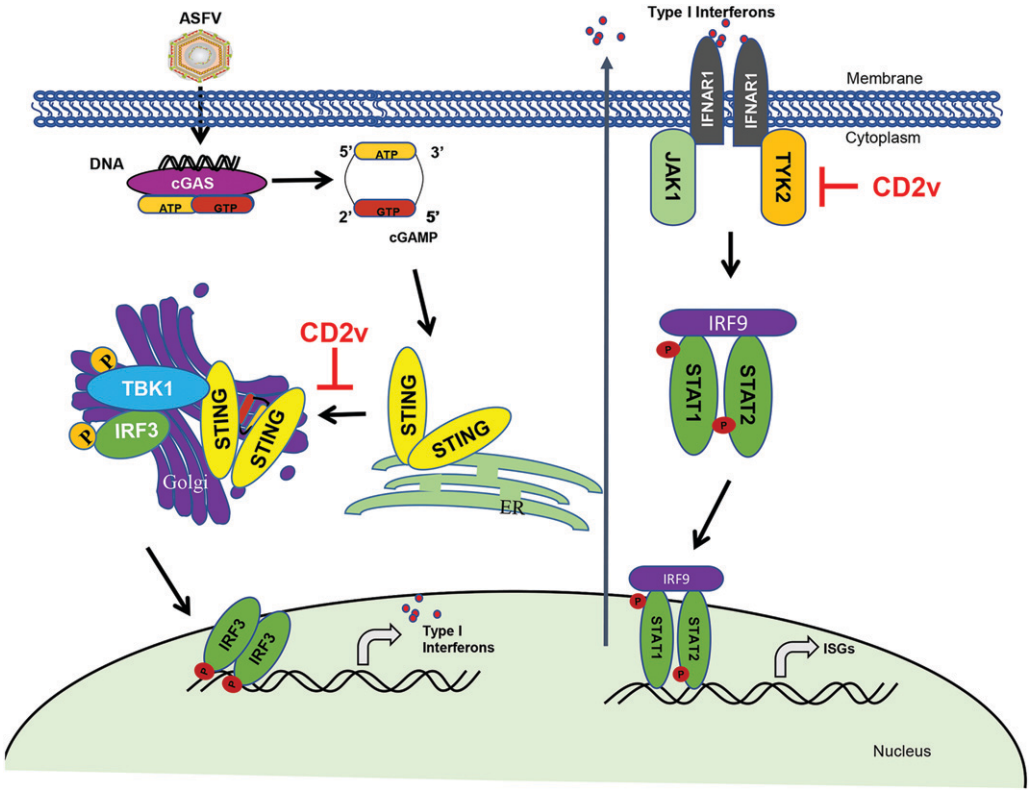

FIGURE 9. A schematic model of ASFV CD2v negatively regulating cGAS-STING and JAK-STAT signaling pathway. On ASFV infection, host cGAS senses the genomic DNA of ASFV to promote the cGAMP production. The cGAMP binds to the ER-localized adaptor protein STING, which leads to transfer from the ER to the Golgi apparatus. Activated STING recruits and phosphorylates TBK1 and IRF3 to promote the production of type I IFNs. Type I IFNs bind to IFNAR1 and IFNAR2, which recruit TYK2 and JAK1, respectively. The activated TYK2 and JAK1 phosphorylate STAT1 and STAT2 and lead to ISG expression. On the one hand, the ASFV CD2v interacts with STING to attenuate its localization on Golgi to inhibit type I IFNs production. On the other hand, ASFV CD2v interacts with IFNAR1 and IFNAR2 to destruct the interactions of IFNAR1-TYK2 and IFNAR2-JAK1 to inhibit ISG production in the IFN signaling pathway.

References

1. Dixon, L. K., H. Sun, and H. Roberts. 2019. African swine fever. *Antiviral Res.* 165: 34–41.
2. Shurson, G. C., A. Palowski, J. L. G. van de Ligt, D. C. Schroeder, C. Balestreri, P. E. Urriola, and F. Sampedro. 2022. New perspectives for evaluating relative risks of African swine fever virus contamination in global feed ingredient supply chains. *Transbound. Emerg. Dis.* 69: 31–56.
3. Malogolovkin, A., and D. Kolbasov. 2019. Genetic and antigenic diversity of African swine fever virus. *Virus Res.* 271: 197673.
4. Dixon, L. K., D. A. Chapman, C. L. Netherton, and C. Upton. 2013. African swine fever virus replication and genomics. *Virus Res.* 173: 3–14.
5. Correia, S., S. Ventura, and R. M. Parkhouse. 2013. Identification and utility of innate immune system evasion mechanisms of ASFV. *Virus Res.* 173: 87–100.
6. Yang, K., Y. Xue, H. Niu, C. Shi, M. Cheng, J. Wang, B. Zou, J. Wang, T. Niu, M. Bao, et al. 2022. African swine fever virus MGF360-11L negatively regulates cGAS-STING-mediated inhibition of type I interferon production. *Vet. Res. (Faisalabad)* 53: 7.
7. Zhuo, Y., Z. Guo, T. Ba, C. Zhang, L. He, C. Zeng, and H. Dai. 2021. African swine fever virus MGF360-12L inhibits type i interferon production by blocking the interaction of importin α and NF-κB signaling pathway. *Virol. Sin.* 36: 176–186.
8. Wang, Y., S. Cui, T. Xin, X. Wang, H. Yu, S. Chen, Y. Jiang, X. Gao, Y. Jiang, X. Guo, et al. 2022. African swine fever virus MGF360-14L negatively regulates type I interferon signaling by targeting IRF3. *Front. Cell. Infect. Microbiol.* 11: 818969.
9. Li, J., J. Song, L. Kang, L. Huang, S. Zhou, L. Hu, J. Zheng, C. Li, X. Zhang, X. He, et al. 2021. pMGF505-7R determines pathogenicity of African swine fever virus infection by inhibiting IL-1β and type I IFN production. *PLoS Pathog.* 17: e1009733.
10. Afonso, C. L., M. E. Piccone, K. M. Zaffuto, J. Neilan, G. F. Kutish, Z. Lu, C. A. Balinsky, T. R. Gibb, T. J. Bean, L. Zsak, and D. L. Rock. 2004. African swine fever virus multigene family 360 and 530 genes affect host interferon response. *J. Virol.* 78: 1858–1864.
11. Phelan, T., M. A. Little, and G. Brady. 2020. Targeting of the cGAS-STING system by DNA viruses. *Biochem. Pharmacol.* 174: 113831.
12. Briard, B., D. E. Place, and T. D. Kanneganti. 2020. DNA sensing in the innate immune response. *Physiology (Bethesda)* 35: 112–124.
13. Taguchi, T., K. Mukai, E. Takaya, and R. Shindo. 2021. STING operation at the ER/Golgi interface. *Front. Immunol.* 12: 646304.
14. Zhang, X., J. Wu, F. Du, H. Xu, L. Sun, Z. Chen, C. A. Brautigam, X. Zhang, and Z. J. Chen. 2014. The cytosolic DNA sensor cGAS forms an oligomeric complex with DNA and undergoes switch-like conformational changes in the activation loop. *Cell Rep.* 6: 421–430.
15. Liu, S., X. Cai, J. Wu, Q. Cong, X. Chen, T. Li, F. Du, J. Ren, Y. T. Wu, N. V. Grishin, and Z. J. Chen. 2015. Phosphorylation of innate immune adaptor proteins MAVS, STING, and TRIF induces IRF3 activation. *Science* 347: aaa2630.
16. Cai, X., Y. H. Chiu, and Z. J. Chen. 2014. The cGAS-cGAMP-STING pathway of cytosolic DNA sensing and signaling. *Mol. Cell* 54: 289–296.
17. Meyts, I., and J. L. Casanova. 2021. Viral infections in humans and mice with genetic deficiencies of the type I IFN response pathway. *Eur. J. Immunol.* 51: 1039–1061.
18. Dixon, L. K., C. C. Abrams, G. Bowick, L. C. Goatley, P. C. Kay-Jackson, D. Chapman, E. Liverani, R. Nix, R. Silk, and F. Zhang. 2004. African swine fever virus proteins involved in evading host defence systems. *Vet. Immunol. Immunopathol.* 100: 117–134.
19. Malogolovkin, A., G. Burmakina, E. R. Tulman, G. Delhon, D. G. Diel, N. Salnikov, G. F. Kutish, D. Kolbasov, and D. L. Rock. 2015. African swine fever virus CD2v and C-type lectin gene loci mediate serological specificity. *J. Gen. Virol.* 96: 866–873.
20. Goatley, L. C., and L. K. Dixon. 2011. Processing and localization of the African swine fever virus CD2v transmembrane protein. *J. Virol.* 85: 3294–3305.
21. Pérez-Núñez, D., E. García-Urdiales, M. Martínez-Bonet, M. L. Nogal, S. Barroso, Y. Revilla, and R. Madrid. 2015. CD2v interacts with adaptor protein AP-1 during African swine fever infection. *PLoS One* 10: e0123714.
22. Kay-Jackson, P. C., L. C. Goatley, L. Cox, J. E. Miskin, R. M. E. Parkhouse, J. Wienands, and L. K. Dixon. 2004. The CD2v protein of African swine fever virus interacts with the actin-binding adaptor protein SH3P7. *J. Gen. Virol.* 85: 119–130.
23. Rodríguez, J. M., R. J. Yáñez, F. Almazán, E. Viñuela, and J. F. Rodriguez. 1993. African swine fever virus encodes a CD2 homolog responsible for the adhesion of erythrocytes to infected cells. *J. Virol.* 67: 5312–5320.
24. Rowlands, R. J., M. M. Duarte, F. Boinas, G. Hutchings, and L. K. Dixon. 2009. The CD2v protein enhances African swine fever virus replication in the tick vector, Ornithodoros erraticus. *Virology* 393: 319–328.
25. Monteagudo, P. L., A. Lacasta, E. López, L. Bosch, J. Collado, S. Pina-Pedrero, F. Correa-Fiz, F. Accensi, M. J. Navas, E. Vidal, et al. 2017. BA71ΔCD2: a new

recombinant live attenuated african swine fever virus with cross-protective capabilities. *J. Virol.* 91: e01058-17.
26. Chaulagain, S., G. A. Delhon, S. Khatiwada, and D. L. Rock. 2021. African swine fever virus CD2v protein induces β-interferon expression and apoptosis in swine peripheral blood mononuclear cells. *Viruses* 13: 1480.
27. Zhao, D., R. Liu, X. Zhang, F. Li, J. Wang, J. Zhang, X. Liu, L. Wang, J. Zhang, X. Wu, et al. 2019. Replication and virulence in pigs of the first African swine fever virus isolated in China. *Emerg. Microbes Infect.* 8: 438–447.
28. Huang, L., H. Liu, K. Zhang, Q. Meng, L. Hu, Y. Zhang, Z. Xiang, J. Li, Y. Yang, Y. Chen, et al. 2020. Ubiquitin-conjugating enzyme 2S enhances viral replication by inhibiting type I IFN production through recruiting USP15 to deubiquitinate TBK1. *Cell Rep.* 32: 108044.
29. King, D. P., S. M. Reid, G. H. Hutchings, S. S. Grierson, P. J. Wilkinson, L. K. Dixon, A. D. Bastos, and T. W. Drew. 2003. Development of a TaqMan PCR assay with internal amplification control for the detection of African swine fever virus. *J. Virol. Methods* 107: 53–61.
30. Rathakrishnan, A., S. Connell, V. Petrovan, K. Moffat, L. C. Goatley, T. Jabbar, P. J. Sánchez-Cordón, A. L. Reis, and L. K. Dixon. 2022. Differential effect of deleting members of african swine fever virus multigene families 360 and 505 from the genotype II Georgia 2007/1 isolate on virus replication, virulence, and induction of protection. *J. Virol.* 96: e0189921.
31. Chen, W., D. Zhao, X. He, R. Liu, Z. Wang, X. Zhang, F. Li, D. Shan, H. Chen, J. Zhang, et al. 2020. A seven-gene-deleted African swine fever virus is safe and effective as a live attenuated vaccine in pigs. *Sci. China Life Sci.* 63: 623–634.
32. García-Belmonte, R., D. Pérez-Núñez, M. Pittau, J. A. Richt, and Y. Revilla. 2019. African swine fever virus Armenia/07 virulent strain controls interferon beta production through the cGAS-STING pathway. *J. Virol.* 93: e02298-18.
33. Huang, L., W. Xu, H. Liu, M. Xue, X. Liu, K. Zhang, L. Hu, J. Li, X. Liu, Z. Xiang, et al. 2021. African swine fever virus pI215L negatively regulates cGAS-STING signaling pathway through recruiting RNF138 to inhibit K63-linked ubiquitination of TBK1. *J. Immunol.* 207: 2754–2769.
34. Lin, R., Y. Mamane, and J. Hiscott. 1999. Structural and functional analysis of interferon regulatory factor 3: localization of the transactivation and autoinhibitory domains. *Mol. Cell. Biol.* 19: 2465–2474.
35. Gui, X., H. Yang, T. Li, X. Tan, P. Shi, M. Li, F. Du, and Z. J. Chen. 2019. Autophagy induction via STING trafficking is a primordial function of the cGAS pathway. *Nature* 567: 262–266.
36. McCrossan, M., M. Windsor, S. Ponnambalam, J. Armstrong, and T. Wileman. 2001. The trans Golgi network is lost from cells infected with African swine fever virus. *J. Virol.* 75: 11755–11765.
37. Ramanjulu, J. M., G. S. Pesiridis, J. Yang, N. Concha, R. Singhaus, S. Y. Zhang, J. L. Tran, P. Moore, S. Lehmann, H. C. Eberl, et al. 2018. Design of amidobenzimidazole STING receptor agonists with systemic activity. [Published erratum appears in 2019 *Nature* 570: e53.] *Nature* 564: 439–443.
38. Teklue, T., T. Wang, Y. Luo, R. Hu, Y. Sun, and H. J. Qiu. 2020. Generation and evaluation of an African swine fever virus mutant with deletion of the *CD2v* and *UK* genes. *Vaccines (Basel)* 8: 763.
39. Gladue, D. P., V. O'Donnell, E. Ramirez-Medina, A. Rai, S. Pruitt, E. A. Vuono, E. Silva, L. Velazquez-Salinas, and M. V. Borca. 2020. Deletion of CD2-like (CD2v) and C-type lectin-like (EP153R) genes from African swine fever virus Georgia-Δ9GL abrogates its effectiveness as an experimental vaccine. *Viruses* 12: 1185.
40. Kato, K., H. Omura, R. Ishitani, and O. Nureki. 2017. Cyclic GMP-AMP as an endogenous second messenger in innate immune signaling by cytosolic DNA. *Annu. Rev. Biochem.* 86: 541–566.
41. Ma, Z., and B. Damania. 2016. The cGAS-STING defense pathway and its counteraction by viruses. *Cell Host Microbe* 19: 150–158.
42. Karger, A., D. Pérez-Núñez, J. Urquiza, P. Hinojar, C. Alonso, F. B. Freitas, Y. Revilla, M. F. Le Potier, and M. Montoya. 2019. An update on African swine fever virology. *Viruses* 11: 864.
43. Zheng, X., S. Nie, and W. H. Feng. 2022. Regulation of antiviral immune response by African swine fever virus (ASFV). *Virol. Sin.* 37: 157–167.
44. de Oliveira, V. L., S. C. Almeida, H. R. Soares, A. Crespo, S. Marshall-Clarke, and R. M. Parkhouse. 2011. A novel TLR3 inhibitor encoded by African swine fever virus (ASFV). *Arch. Virol.* 156: 597–609.
45. Henriques, E. S., R. M. Brito, H. Soares, S. Ventura, V. L. de Oliveira, and R. M. Parkhouse. 2011. Modeling of the Toll-like receptor 3 and a putative Toll-like receptor 3 antagonist encoded by the African swine fever virus. *Protein Sci.* 20: 247–255.
46. Li, D., W. Yang, L. Li, P. Li, Z. Ma, J. Zhang, X. Qi, J. Ren, Y. Ru, Q. Niu, et al. 2021. African swine fever virus MGF-505-7R negatively regulates cGAS-STING-mediated signaling pathway. *J. Immunol.* 206: 1844–1857.
47. Liu, H., Z. Zhu, T. Feng, Z. Ma, Q. Xue, P. Wu, P. Li, S. Li, F. Yang, W. Cao, et al. 2021. African swine fever virus E120R protein inhibits interferon beta production by interacting with IRF3 to block its activation. *J. Virol.* 95: e0082421.
48. Li, D., J. Zhang, W. Yang, P. Li, Y. Ru, W. Kang, L. Li, Y. Ran, and H. Zheng. 2021. African swine fever virus protein MGF-505-7R promotes virulence and pathogenesis by inhibiting JAK1- and JAK2-mediated signaling. *J. Biol. Chem.* 297: 101190.
49. Zhang, K., B. Yang, C. Shen, T. Zhang, Y. Hao, D. Zhang, H. Liu, X. Shi, G. Li, J. Yang, et al. 2022. MGF360-9L is a major virulence factor associated with the African swine fever virus by antagonizing the JAK/STAT signaling pathway. *MBio* 13: e0233021.